The 2010 IEEE/RSJ International Conference on
Intelligent Robots and Systems
October 18-22, 2010, Taipei, Taiwan

A New Sonar Salient Feature Structure for EKF-based SLAM

Se-Jin Lee and Jae-Bok Song

Abstract—Not all line or point features capable of being extracted by sonar sensors from cluttered home environments are useful for simultaneous localization and mapping (SLAM) due to their ambiguity. We present a new sonar feature structure suitable for a cluttered environment and the extended Kalman filter (EKF)-based SLAM scheme. The key concept is to extract circle feature clouds on salient convex objects by sonar data association. The centroid of each circle cloud, called a sonar salient feature, is used as a natural landmark for EKF-based SLAM. After completing initial exploration in an unknown environment, SLAM-able areas with sonar salient features can be defined, and cylindrical objects are placed conveniently at weak SLAM-able areas as a supplemental environmental saliency to enhance SLAM performance. Experimental results demonstrate the validity and robustness of the proposed sonar salient feature structure for EKF-based SLAM.

I. Introduction

AUTONOMOUS navigation of a mobile robot requires the integration of motion control, mapping, and localization. When a mobile robot is in an unknown environment, it needs to build a map of its environment incrementally while simultaneously determining its location on the map. This process is called simultaneous localization and mapping (SLAM) [1]. The difficulty of SLAM lies in the fact that its two components of mapping and localization are strongly correlated. Considerable research has been done on theoretical SLAM algorithms with range sensors [2]-[5].

A mobile robot uses various sensors including vision sensors and range sensors (e.g., sonar sensors, laser scanners, and infrared sensors). Sonar sensors are widely used in many commercial applications for several reasons. They are much less expensive than other range sensors such as laser scanners and range cameras. The detection ability of a camera is particularly poor for transparent objects or in a dark environment, whereas a sonar sensor works well under such conditions. Moreover, except for outliers caused by specular reflection and crosstalk of sonar sensors, typical sonar sensors can give accurate range data [6].

A sonar sensor, however, has difficulty determining the exact locations of objects because of its wide beam width and sometimes specular reflection. Therefore, several techniques have been developed to improve angular resolution and reduce frequent outliers in a set of sonar data for successful extraction of line and point features. Regions of constant depth (RCDs) were defined from densely scanned data obtained by a rotating sonar sensor at the stationary position for feature extraction [7], [8]. Triangulation-based fusion based on sonar data was presented for the localization of a robot [6]. The Hough transform was used to find a group of sonar arcs tangent to the same line or intersecting at the same point for SLAM [5]. And, a delayed classification algorithm was introduced to categorize planes, corners, and edges for the SLAM process using echo signal processing [9].

As previously mentioned, line and point features have been used to build a map and localize a robot pose from a set of sonar data. However, it is difficult to determine the correspondence of line or point features with previously registered features because of the ambiguity existing in a cluttered home environment. That is, recognizing home environments using line and point features obtained from sonar data often leads to poor SLAM performance in the actual environment [10]. Therefore, a new type of robust sonar feature structure is required for a practical SLAM solution based on sonar sensors.

In this study, we propose a new type of sonar feature called the "sonar salient feature." The key concept is to extract circle clouds on salient convex objects in the environment by associating sets of sonar data. The sonar salient features are applied to the extended Kalman filter (EKF)-based SLAM framework as a natural landmark. Moreover, analyzing the initial feature map, we searched for weak SLAM-able areas for sonar salient features and placed simple cylindrical objects there to create abundant environmental saliencies. Our experimental results demonstrate the validity and robustness of the sonar salient feature structure for EKF-based SLAM.

The rest of the paper is organized as follows. Section 2 presents the details of the sonar salient feature. Section 3 discusses how the sonar salient features are combined with the EKF-based SLAM scheme, and Section 4 presents experimental results of SLAM based on sonar salient features. The conclusion is given in Section 5.

II. Sonar Salient Feature

A. Footprint Association (*FPA*) Model

To verify the reliability of each sonar data set and extract geometric features from each set, we need a data interpretation filter. A footprint association (FPA) model [11] was used in this study. The FPA model basically determines whether or not two sonar data points measured at different robot poses originate from the same hypothetical object.

In Fig. 1, the two circles centered at sensor locations (o_1, o_2) are defined with their radii equal to the range values (z_1, z_2).

Se-Jin Lee is with the Intelligent Robotics Research Center, Korea University, and the Department of Mechanical Engineering, Seoul National University of Technology, Seoul, Korea (e-mail: sejiny3@gmail.com).

Jae-Bok Song (corresponding author) is with the School of Mechanical Engineering, Korea University, Seoul, Korea (phone: +82-2-3290-3363, fax: +82-2-3290-3757, e-mail: jbsong@korea.ac.kr).

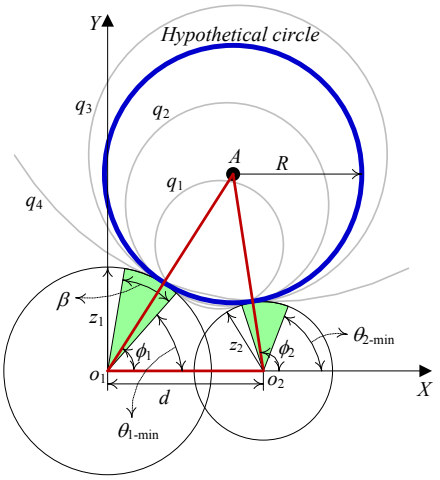

Fig. 1. Geometric relationship between two individual sonar measurements from different sensor poses.

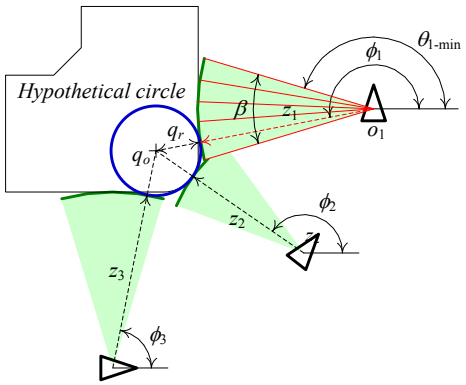

Fig. 2. Example of the specific hypothetical circle satisfying the geometric constraints from three individual sonar footprints.

The angular constraint of each footprint is defined from the sensor direction and the effective beam width β that is represented by the green fan shapes in Fig. 1. Without loss of generality, we considered a local coordinate frame centered at sensor location 1 (o_1) with sensor location 2 (o_2) on the positive x-axis at position $x = d$, where d is the distance between the two sensor locations. The angles (ϕ_1, ϕ_2) are the bearings from the positive x-axis of the local coordinate frame to the center A of a hypothetical circle. Using the second law of cosines, we obtained the following relationship between R and ϕ_1:

$$\cos(\phi_1) = \frac{(z_1 + R)^2 - (z_2 + R)^2 + d^2}{2d(z_1 + R)} \tag{1}$$

where angle ϕ_1 must satisfy its angular constraint

$$\theta_{1\text{–min}} \le \phi_1 \le \theta_{1\text{–min}} + \beta. \tag{2}$$

Radius R was derived from Eq. (1):

$$R = \frac{(z_1)^2 - (z_2)^2 - 2d\cos(\phi_1)z_1 + d^2}{2(d\cos(\phi_1) + z_2 - z_1)}. \tag{3}$$

With radius R from Eq. (3), we obtained the angle ϕ_2:

$$\phi_2 = \pi - \cos^{-1}\left(\frac{(z_2 + R)^2 - (z_1 + R)^2 + d^2}{2d(z_2 + R)}\right) \tag{4}$$

and angle ϕ_2 must also satisfy its angular constraint

$$\theta_{2\text{–min}} \le \phi_2 \le \theta_{2\text{–min}} + \beta. \tag{5}$$

Satisfaction of the angular constraint by ϕ_2 indicates that these sonar data were reflected from the same object. However, we cannot determine the values of R uniquely because the angle ϕ_1 cannot be uniquely determined within its wide beam width. Two sets of sonar data can generate innumerable hypothetical circles that satisfy the angular constraints of both sonar sensors (e.g., four tangent circles q_1, … , q_4 in Fig. 1). To deal with this problem, we divided the first sonar footprint centered at o_1 into several angular segments (represented by red lines) to determine their tangent circles, as shown in Fig. 2.

B. Convex Saliency Circling

We considered three sonar footprints to find the unique and reliable hypothetical circle, as shown in Fig. 2. The angle ϕ_1 is one of the angles divided within the effective beam width of the first sonar footprint. The radius q_r of the tangent circle, and its corresponding angle ϕ_2 of the second sonar footprint, was calculated between both sonar footprints using the FPA model. The angle ϕ_2 must satisfy the angular constraint described in Eq. (5). Next, we geometrically associated this hypothetical circle with the third footprint F_3. If the angle ϕ_3 corresponding to the hypothetical circle satisfies its angular constraint, this circle feature is qualified and is finally registered in storage.

The convex saliency circling algorithm is implemented by the pseudocode listed in Table 1, and the example of four hypothetical circles from three arbitrary sonar footprints is shown in Fig. 3. An explanation for each line of Table 1 is given as follows:

(a) Select the first sonar footprint (o_i, z_i, $\theta_{i\text{-min}}$) from the stored sonar data. The variable m is the number of sonar sensors mounted on the robot and n is the number of data collections in the data storage. Therefore, the total number of sonar data in the storage is m x n (in this study, m = 12 and n = 25).

(b) Check if the sonar data z_i is within the acceptable range (r_{min}, r_{max}) of a sonar sensor, where r_{min} and r_{max} are the minimum and maximum ranges (r_{min} = 0.05 m and r_{max} = 4.0 m).

(c) Select the second sonar footprint (o_j, z_j, $\theta_{j\text{-min}}$) from storage.

TABLE I
PSEUDOCODE: CONVEX SALIENCY CIRCLING

for $i = 1 \rightarrow m \times n$	(a)
if $r_{min} < z_i < r_{max}$	(b)
for $j = i+1 \rightarrow m \times n$	(c)
if $r_{min} < z_j < r_{max}$	(d)
for $\phi_i = \theta_{i\text{-min}} \rightarrow \theta_{i\text{-min}} + \beta$, $\phi_i = \phi_i + \delta$	(e)
FPA model {In : (o_i, z_i, $\theta_{i\text{-min}}$), (o_j, z_j, $\theta_{j\text{-min}}$), ϕ_i ; Out: (q_o, q_r)}	(f)
if $p_{min} < q_r < p_{max}$	(g)
for $k = j+1 \rightarrow m \times n$	(h)
if $\lvert D-q_r-z_k \rvert < \sigma$	(i)
$C = [C; q_o\ q_r]$	(j)

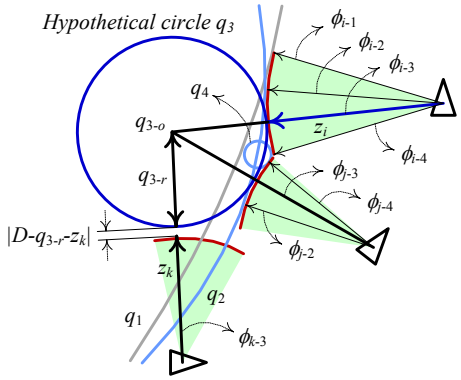

Fig. 3. Example of four hypothetical circles from the convex saliency circling process.

(d) Check if the sonar data z_j is within the acceptable range.

(e) Divide the first sonar footprint into $\beta/\delta+1$ segments, where β is the effective beam width and δ is the angular increment. Assuming that β = 30° and δ = 10°, we obtained four angular segments ϕ_{i-1}, … , ϕ_{i-4} from the first sonar data as shown in Fig. 3.

(f) In the FPA model function, the inputs are the first and second sonar footprints. One of ϕ_{i-1}, … , ϕ_{i-4}, and the output is the hypothetical circle feature q represented by center position q_o and radius q_r. Four hypothetical circles are shown in Fig. 3. The circle q_1 tangent to the angle ϕ_{i-1} is eliminated by the FPA model because it does not satisfy Eq. (5). In the example shown in Fig. 3, the other circles are accepted.

(g) Check if the radius of the hypothetical circle is within the threshold range of (p_{min}, p_{max}), where p_{min} and p_{max} are the minimum and maximum thresholds (p_{min} = 0.03 m and p_{max} = 0.3 m).

(h) Select the third sonar footprint (o_k, z_k, $\theta_{k\text{-min}}$) from storage.

(i) Check if the third footprint is tangent to the hypothetical circle within a gap tolerance of σ, where D is the distance between the sonar sensor location and the center of the circle (σ=0.02 m in this study). Only q_3 is qualified in the example of Fig. 3.

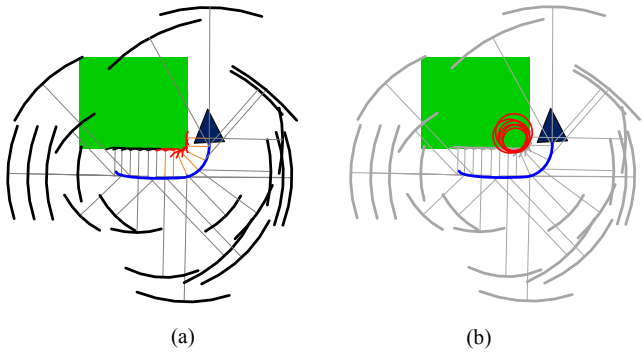

Fig. 4. Example of extraction of sonar salient feature: (a) all sonar footprints in the storage, and (b) the circle cloud obtained by the convex saliency circling process.

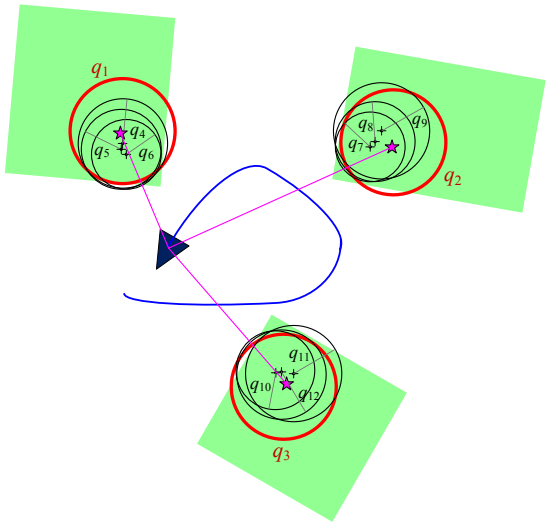

Fig. 5. Example of classification of circles extracted by the convex saliency circling process and the sonar salient features defined as a centroid of circles of each group.

(j) Finally, if all the preceding conditions are met, this circle feature is saved in storage C.

C. Sonar Salient Features

A sonar data stack can include several sets of three sonar data which extract circle features at the salient corners of the environment. For example, Fig. 4(a) shows all sonar footprints in the data storage. A convex corner around the robot trajectory was detected by several sonar data colored in red. Figure 4(b) shows the result of circle cloud extracted by the proposed convex saliency circling process using sonar data.

The next step is a classification of circles corresponding to each salient region of the environment. Assuming that storage C includes the circles q_1, … , q_{12} as shown in Fig. 5, we can locally select the largest circles q_1, q_2, and q_3, colored in red. Then, these largest circles search for their own circles whose center is within the inside of q_1, q_2, and q_3. In the example of Fig. 5, the circles q_4, q_5, and q_6 are grouped by q_1. In the same way, the circles q_7, q_8, and q_9 can be grouped by q_2 and the

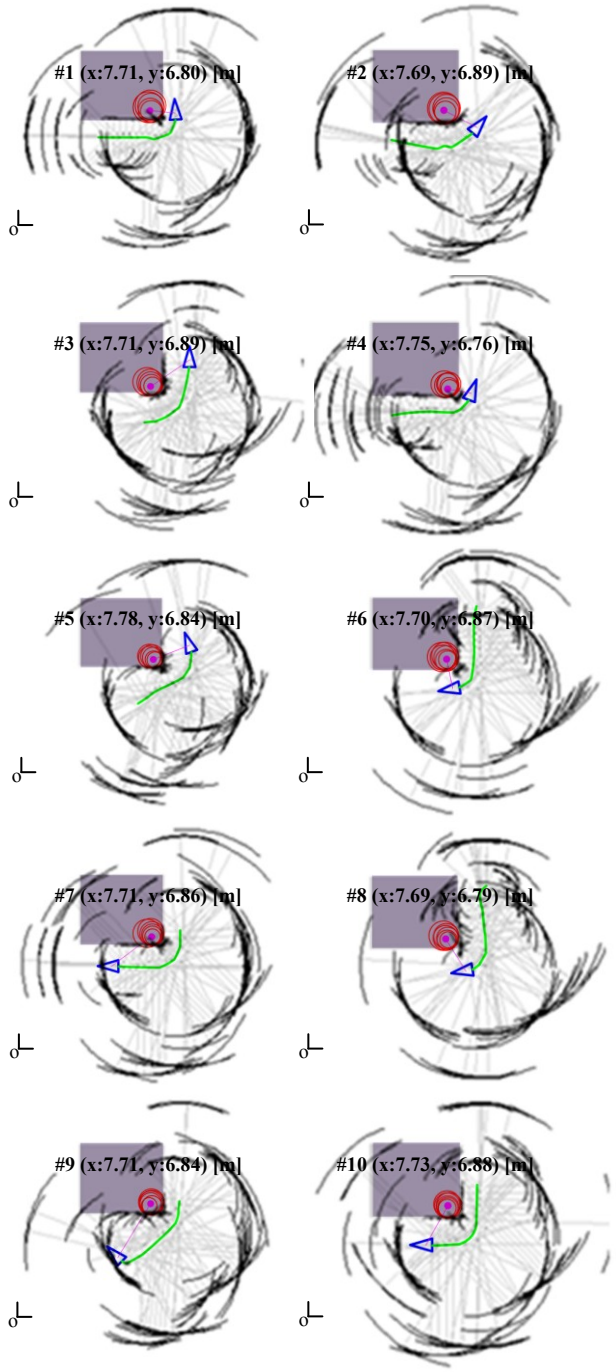

Fig. 6. Results of circle clouds extracted by convex saliency circling on ten different explorations at the same corner (fabric sofa). Each result shows all sonar footprints stored in the sliding data window and extracted circle clouds and its centroid.

circles q_{10}, q_{11}, and q_{12} by q_3. The number of circles in each group indicates the certainty of corner saliency, and the group is eliminated if it does not have more than a certain number of circle elements. The star marks in Fig. 5 indicate a centroid of circles of each group, and they are used as the sonar salient feature. Therefore, the classification of circles can be performed by the aforementioned simple geometric condition. To evaluate the precision of sonar salient feature extracted by the convex saliency circling process, we conducted a series of experiments at the same corner with different trajectories. Figure 6 shows the results of circle clouds and its centroid for ten different explorations. The mean position (x, y) of the sonar salient features was (7.72 m, 6.84 m) and its standard deviation was (0.03 m, 0.04 m).

III. EKF SLAM

A. Map States

The earliest SLAM algorithm was based on an extended Kalman filter (EKF) framework, which is a Bayes filter that represents posteriors with Gaussians that are unimodal distributions. These can be represented compactly by a small number of parameters. The EKF-based SLAM algorithm applies the EKF to online SLAM using maximum likelihood data association for the correspondence test of features. The feature map consists of sonar salient features for landmarks. In stochastic mapping, the environmental information is represented by a global map (X, P):

$$X = \begin{bmatrix} X_{E_0} \\ \vdots \\ X_{En} \end{bmatrix} \quad \text{and} \quad P = \begin{bmatrix} P_{E_0E_0} & \cdots & P_{E_0E_n} \\ \vdots & \ddots & \vdots \\ P_{E_nE_0} & \cdots & P_{E_nE_n} \end{bmatrix}. \tag{6}$$

where the state vector $X = (x_v, y_v, \theta_v, x_1, y_1, \ldots, x_n, y_n)$ contains the estimated locations of the robot E_0 and the sonar salient features $E_1, E_2, \ldots, E_n$, and the matrix P is the error covariance matrix of X. These states are predicted with the robot motion model in the EKF prediction stage, and also estimated with the observations in the EKF update stage. The EKF for SLAM is detailed in [1], [5], [10]. The map is initially empty except for knowledge of the robot pose $X_{E0} = (0, 0, 0)^T$, $P_{E0E0} = 0$.

The robot motion model $g(u)$ for the differential drive robot used in this study is

$$g(u) = \begin{bmatrix} \frac{R(\omega_r + \omega_l)}{2} \Delta T \cdot \cos(\theta_v) \\ \frac{R(\omega_r + \omega_l)}{2} \Delta T \cdot \sin(\theta_v) \\ \frac{R(\omega_r - \omega_l)}{b} \Delta T \end{bmatrix} \tag{7}$$

where u is the control vector composed of two wheel velocities for the robot motion, ω_r and ω_l are the angular velocities of the right and left wheels, ΔT is the time step, r is the wheel radius, and b is the baseline length between two wheels.

A newly observed sonar salient feature was added to the map. We augmented the old state vector and covariance matrix with a new observation $z(\rho^r, \rho^\theta)$ written in the robot's local frame as follows:

$$X^* = \begin{bmatrix} X \\ y(\hat{X}_{E_0}, z) \end{bmatrix} = \begin{bmatrix} X \\ x_v + \rho^r \cos(\rho^\theta + \theta_v) \\ y_v + \rho^r \sin(\rho^\theta + \theta_v) \end{bmatrix} \tag{8}$$

$$P^* = \begin{bmatrix} P & P \cdot Y_v^T \\ Y_v \cdot P & Y_v \cdot P_{E_0 E_0} \cdot Y_v^T + Y_z \cdot R \cdot Y_z^T \end{bmatrix} \quad (9)$$

where X^* is the augmented state vector and R is the 2×2 covariance matrix composed of measurement noise deviations σ_r and σ_θ of the sonar salient feature. Y_v and Y_z are the Jacobian matrices of the feature initialization function $y(\hat{X}_{E_0}, z)$ and are defined as follows:

$$Y_v = \frac{\partial y(\hat{X}_{E_0}, z)}{\partial X_{E_0}} \quad \text{and} \quad Y_z = \frac{\partial y(\hat{X}_{E_0}, z)}{\partial z}. \quad (10)$$

IV. Experimental Results

For the experiments, the Pioneer-3DX differential drive type robot shown in Fig. 7(a) was used. 12 Polaroid sonar sensors, each with a beam width of 15°, were activated selectively as shown in Fig. 7(b) during the exploration. The robot explored the home environment, and was controlled manually at an average speed of 0.2 m/s. During this exploration phase, the sonar ring acquired range data at a frequency of 1 Hz.

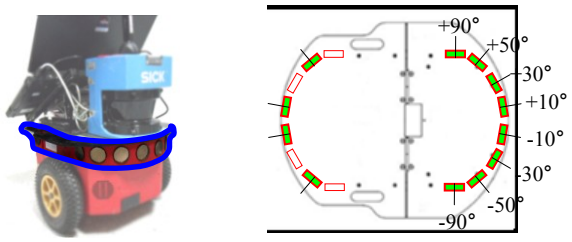

(a) (b)

Fig. 7. Robot platforms. (a) Pioneer-3DX mobile robot equipped with Polaroid sonar sensors, and (b) top view of Pioneer-3DX marked with small lattices of sonar sensors.

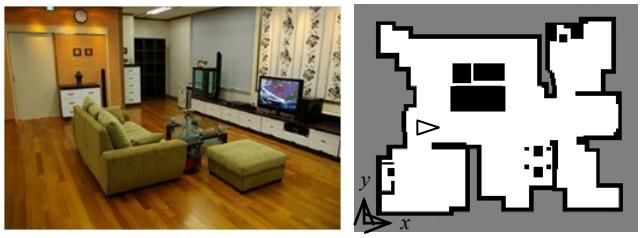

(a) (b)

Fig. 8. Experimental home environment: (a) photo of the home environment, and (b) its CAD map.

The robot carried out a guided exploration in a 12 m × 10 m real home environment as shown in Fig. 8. This environment was composed of three rooms, a kitchen, and a living room including a sofa, wardrobe, bookshelf, bed, table, chair, etc.

Before confirming the usefulness of a sonar salient feature map, we need to investigate the results of the line and point feature maps for a comparison of their clarity of environmental description. In particular, a sonar sensor frequently extracts uncertain or wrong line or point features in a cluttered home environment because of environmental ambiguity and its wide beam width. The use of these line and point features leads to poor SLAM performance. Figure 9 shows sonar line and point features extracted with the initial part of odometric trajectories, which were overlapped over the CAD map. The line and point features were extracted by the method introduced in [11]. In the cases shown in Figs. 9(a) and (b), line features B and D (colored in red) were different from registered features A and C, respectively, but they were associated with the same features due to their environmental ambiguity. In fact the uneven surface and gap of furniture with knobs are not visible in Figs. 9(c) and (d) because of their low bitmap scale, but these knobs and gap can exist anywhere in home environments, which misleads the correspondence test of a point feature. Therefore, these sonar line and point features, some of which are wrong by incorrect data association due to the environmental ambiguity, are obviously inappropriate for SLAM in a cluttered environment.

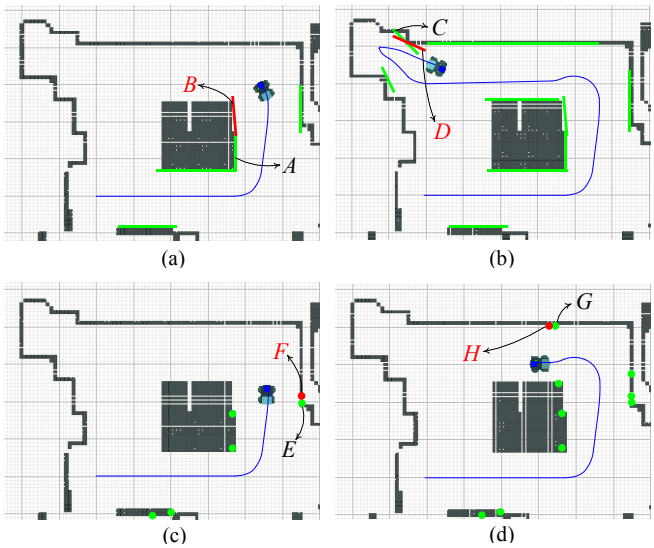

(a) (b) (c) (d)

Fig. 9. Cases causing failure of EKF SLAM in (a,b) line and (c,d) point feature maps built by sonar data.

The total exploration time of the robot was 25 min for a demonstration of the validity of EKF SLAM with sonar salient features. In real-time implementation, the calculation time for sonar salient feature extraction and EKF SLAM on a Pentium IV (2.6 GHz) personal computer was about 0.35 s and 0.01 s, respectively. Figure 10 shows the sonar salient feature map built after all explorations. This feature map was overlapped on the CAD map with odometric trajectories (represented by a blue line). These odometric trajectories drifted due to systematic and random errors. The red line indicates a trajectory estimated by the SLAM process with several sonar salient features (represented by a green lattice). All extracted features corresponded to the convex saliencies of the given environment. As expected, the robot corrected its pose by building a consistent map of its environment incrementally while simultaneously determining its own locations on this map.

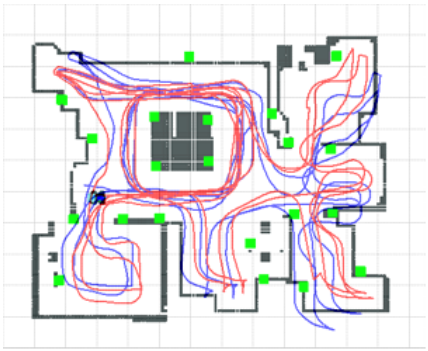

Fig. 10. Sonar salient feature map built after all explorations and its overlap on the CAD map.

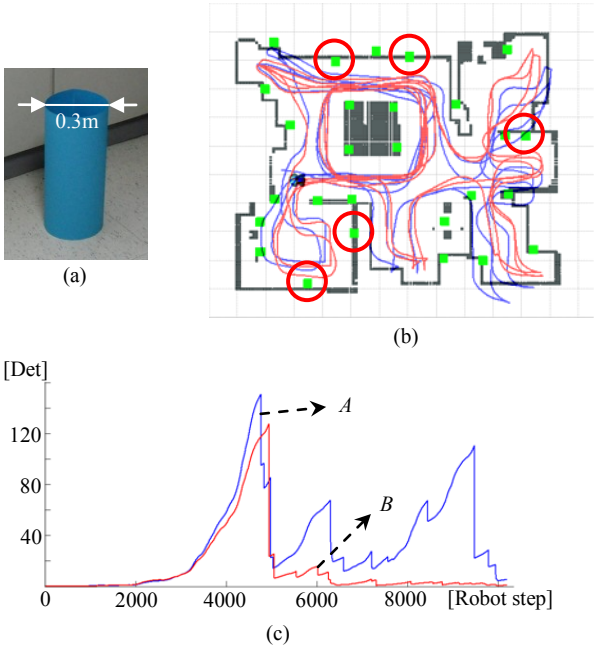

Fig. 11. Experimental results: (a) the cylindrical landmark made of cardboard for weak SLAM-able areas, (b) sonar salient feature map built after all explorations with cylindrical landmarks, and (c) plots of the determinants of the robot pose covariance for exploration in the original environment and in the environment including cylindrical landmarks.

However, there can be weak SLAM-able areas for sonar salient features as shown in Fig. 10. To enhance the convex saliency of the environment for more dependable SLAM performance, we placed several cylindrical objects at weak SLAM-able areas that were selected intuitively. The five artificial landmarks (cylinders made of cardboard as shown in Fig. 11(a)) are marked on the map shown in Fig. 11(b). To further analyze SLAM consistency, the determinants of the robot pose covariance were plotted in Fig. 11(c) for exploration in the original environment (case *A*) and in the environment including artificial landmarks (case *B*). We note that the determinant of case *B* was smaller than that of case *A* after the second half of the time period, as shown in Fig. 11(c). This means that SLAM performance in the environment with five cylindrical landmarks placed at weak SLAM-able areas improved stability.

V. Conclusion

We proposed a method for extracting a new sonar feature structure called the sonar salient feature. The sonar salient feature can serve as a good natural landmark for SLAM using sonar sensors in a cluttered home environment. The SLAM performance in the environment with cylindrical landmarks placed conveniently at weak SLAM-able areas was more stable than that without them. The proposed SLAM scheme based on sonar salient features is applicable to navigation of indoor service robots equipped with sonar sensors.

Acknowledgment

This research was financially supported by the Intelligent Robotics Development Program, one of the 21st Century Frontier R&D Programs funded by the Ministry of Knowledge Economy of the government of Korea.

References

[1] H. F. Durrant-Whyte and T. Bailey, "Simultaneous localization and mapping: part I," IEEE Robotics & Automation Magazine, vol. 13, no. 2, pp. 99-110, 2006.

[2] A. J. Davison, "Real-time simultaneous localisation and mapping with a single camera," Proc. of IEEE International Conference on Computer Vision, pp. 1403-1410, 2003.

[3] C. Kim, R. Sakthivel, and W. K. Chung, "Unscented FastSLAM: A Robust Algorithm for the Simultaneous Localization and Mapping Problem," Proc. of IEEE International Conference on Robotics and Automation, pp. 2439-2445, 2007.

[4] M. Montemerlo and S. Thrun, "Simultaneous localization and mapping with unknown data association using FastSLAM," Proc. of IEEE International Conference on Robotics and Automation, pp. 1985-1991, 2003.

[5] J. D. Tardos, J. Neira, P. M. Newman, and J. J. Leonard, "Robust Mapping and Localization in Indoor Environments Using Sonar Data," The International Journal of Robotics Research, vol. 21, no. 4, pp. 311-330, 2002.

[6] O. Wijk and H. I. Christensen, "Triangulation-Based Fusion of Sonar Data with Application in Robot Pose Tracking," IEEE Transactions on Robotics and Automation, vol. 16, no. 6, pp. 740-752, 2000.

[7] J. J. Leonard and H. F. Durrant-Whyte, "Mobile Robot Localization by Tracking Geometric Beacons," IEEE Transactions on Robotics and Automation, vol. 7, no. 3, pp. 376-382, 1991.

[8] J. J. Leonard and H. F. Durrant-Whyte, "Directed Sonar Sensing for Mobile Robot Navigation," Kluwer Academic Publishers, Massachusetts, 1992.

[9] S. Fazli and L. Kleeman, "Simultaneous landmark classification, localization and map building for an advanced sonar ring," Robotica, vol. 25, no. 3, pp. 283-296, 2007.

[10] S.-J. Lee, "Development of Robust Environmental Feature Structure for SLAM in Indoor Environments Using Sonar Sensors," Ph.D. thesis, Pohang University of Science and Technology of Korea, 2009.

[11] S.-J. Lee, J.-H. Lim, and D.-W. Cho, "Robust Feature Detection for Mapping and Localization of a Mobile Robot Using Sparsely Sampled Sonar Data," Advanced Robotics, vol. 23, no. 12-13 pp. 1601-1616, 2009.